Heat Load Budgeting of a Superconducting Induction Heater's Commercial Cryocooler-Based Cryostat

M.Sc. Lennard Busch[*], Dr.-Ing. Ralph Lietzow,
Dr.-Ing. Holger Neumann

Karlsruhe Institute of Technology (KIT)
Institute of Technical Physics (ITEP)
76344 Eggenstein-Leopoldshafen
Germany

lennard.busch@kit.edu, ralph.lietzow@kit.edu, holger.neumann@kit.edu

*Corresponding Author

Abstract

Within a project funded by the German Federal Ministry for Economic Affairs and Energy (BMWI), the Karlsruhe Institute of Technology (KIT) collaborates with the Theva GmbH and Bültmann GmbH to develop a superconducting magnetic heater. The Theva GmbH designs and supplies the high-temperature superconducting (HTS) coil. It will be integrated in a cryostat designed and supplied by KIT and cooled to ca. 25 K via a GM-cryocooler. Granted successful test results at KIT, the cryostat with the superconducting coil will serve to operate an induction heater at the Bültmann GmbH and be assessed there under industrial conditions. The challenge within the cryogenic design lies in the simultaneous requirement of relatively low production costs, robustness and extremely limited operation downtimes to form a competitive product.

This contribution presents aspects of the cryogenic system's conceptional design, with a focus on its heat load budgeting. Due to the limited cooling capacities of cryocoolers on each stage, the main aim of the design is to distribute the estimated heat loads as suitably as possible between the cryocooler stages. In the cryostat we designed, the total heat loads on both cryocooler stages will have three significant contributions: heat conduction along connected components, Joule heating and thermal radiation. The respective estimation methods for these heat loads and their results are briefly shown and evaluated in this contribution. In this context, specific examples for the results' influence on the cryostat design within the scope of thermal and economical design are given. The heat load approximations' eligibility to serve as a determination basis of an appropriate cryocooler model is discussed as well. On this basis, finally, we give suggestions for specific cryocooler models currently on the market.

Key Words:

Cryogenics, Cryostat, Cryocooler, Heat Load, Superconductivity

1   Introduction

The most common manufacturing process of finished and semi-finished metal products has always been and is still the hot forming. Aluminum, in this context, needs to be warmed up to around 500 °C before it can be extruded into various shapes. This is nowadays often achieved by induction heaters based on water-cooled normal-conducting inductors. To significantly improve their energy efficiency by ca. 30 %, the inductors can be made out of high-temperature superconductors [1]. Considering the total annual German aluminum extrusion press throughput of ca. 600 kilotons [2], this alone corresponds to an electric energy saving potential of ca. 75 GWha^{-1}. Clearly, the use of superconductors calls for the integration of the induction coils into a cryogenic system. Potential buyers normally argue that an installation of a rather fragile Helium infrastructure in the surroundings of large-scale metal processing industry is impracticable, economically inefficient and therefore unwanted. The cooling power within this system is therefore to be provided by cryocoolers. The main aim of the project is to prove the feasibility of designing and constructing such a superconducting induction heater in a sufficiently cost-effective way in order to lastingly introduce the HTS-technology to the market.

The general feasibility of constructing an industrial-scale superconducting induction heater with a cryocooler-based cryogenic system has already been shown ([3], [4]). However, the creation of a commercially profitable system with long-term operation reliability has yet to be achieved. In the past months, the KIT collaborated with the Theva GmbH and the Bültmann GmbH within a BMWI-funded project to design such a system. The present contribution exclusively focuses on the respective cryogenic system's design.

2   Cryostat Baseline Design Properties

For a better understanding of the overall heat load budgeting, first, we briefly present the cryostat design properties that previously resulted from more generalized contemplation and pre-existing boundary conditions.

2.1   Cryostat Outer Dimensions

An existing iron yoke was to be used to direct the magnetic field lines appropriately through the metal billets to be warmed up. This led to a strongly limited length, width and height of the cryostat's vacuum vessel the horizontal base shape of which is a hollow rectangle as Fig. 1 c) shows.
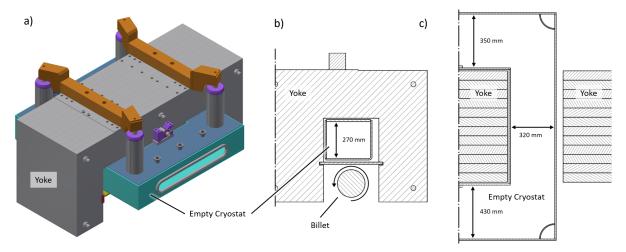

Fig. 1: Different yoke and vacuum vessel views: a) 3D-rendered, isometric view, b) one-sided vertical cross section with indicated rotating metal billet, c) one-sided horizontal cross section.

The resulting inner dimensions of the rectangular cryostat arm's vertical cross section as seen in Fig. 1 b) are 320…430 · 270 mm depending on the respective side of the cryostat. Overall, the horizontal outer dimensions of the cryostat are 1650 · 1400 mm.

2.2   Thermal Baseline Design

Another key baseline design aspect is the use of a thermal shield around the HTS-coil at the intermediate temperature of 80 K. We discuss the decision to apply the shield in another publication [5]. One of the main arguments in favor of an intermediate shield application is related to the fact that we will have to have the required cooling power generated by cryocoolers. The induction heater will be required to operate in the harsh environments of the large-scale metal processing industry. Plus, the use of a coil comprised of a third generation HTS to provide a sufficiently strong magnetic field for the induction heater calls for an operational temperature of ca. 25 K. Thus, to provide cooling power at this low temperature level for the HTS, we expect potential customers to be reluctant to relying on a He-infrastructure. Cryocoolers represent a simpler integration possibility of the induction heater into the metal processing chains of customers. To provide cooling power at two different temperature levels (80 K and 20 K), we chose to use a double-stage GM-cryocooler. We based this decision mainly on production- and operating cost (higher efficiency and consequently lower energy consumption of a two-stage cooler than for a single-stage cooler) considerations of the whole system. Furthermore, a solution with pulse tube cryocoolers and/or two single-stage cryocoolers would exhibit unwanted shorter maintenance intervals. This is a crucial argument for customers that operate continuous metal processing lines.

3   Design Methods and Examples

We used multiple methods and resources to determine the cryostat design. The design needs to comply with a highly competitive manufacturing cost budget and, accordingly, low heat loads on both the thermal shield at 80 K and the HTS-coil at 25 K. Simultaneously, it has to maintain structural integrity. In this section, we present these design methods including examples.

3.1   CAD Software

Throughout the entire design process of the cryostat, we used computer-aided design (CAD) software. Generally, we started from simplified models of single parts. This allowed for mechanical and thermal eligibility calculations and thus the choice of material. From that point, the parts underwent revision, if necessary, and were finished after detail engineering. One example are the pressure support struts which keep the coil in position, mainly by providing support against the large vertical electromagnetic forces on the coil. One of the four struts is displayed in Fig. 2.
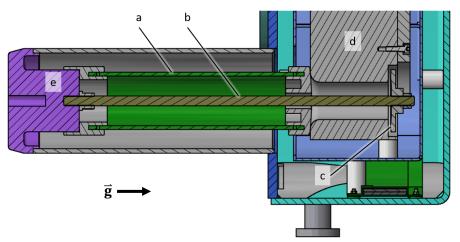

Fig. 2: Vertical cryostat cross section including G10-support strut (a), Titanium suspension rod (b), stainless steel support plate (c), HTS-coil steel case (d) and vacuum vessel dome (e) in operational state.

The support strut design displayed in Fig. 2 has two main beneficial features. First, it provides special efficiency since it hosts the G10 pressure support strut (a) in the same vacuum vessel dome (e) as the Titanium suspension rod (b). Second, the design takes advantage of the fact that once current flows through the HTS-coil, the occurring electromagnetic (EM) forces pull on the coil in opposite direction to the gravitation. The EM-forces are higher than the entire coil's weight. Thus, by providing merely a few millimetres of clearance between the coil casing's top and the pressure support's bottom during assembly, the coil will lift itself up against the G10-strut when

electric flow is induced and the contact to the stainless steel support plate is broken. This guarantees that the cold HTS-coil is exclusively in contact with one of these two heat conductors connected to the 300 K vessel (e) at any given point. During cooldown, it sits on the plate attached to the Titanium-rod and in magnet operation, it presses against the G10-strut, reducing the parasitic heat loads via conduction. The same effect is brought into play by rounding the fit edges of the pressure support strut in the coil casing. The resulting increased coil position stability caused by the strong EM-forces is so high that the installation of further horizontal support for the coil is not imperative.

Another example for the use of CAD-software in the design process is the cold bus thermally linking the cold finger's second stage with the HTS-coil. It allows for heat discharge from the superconductor. The respective installation model can be seen in Fig. 3.
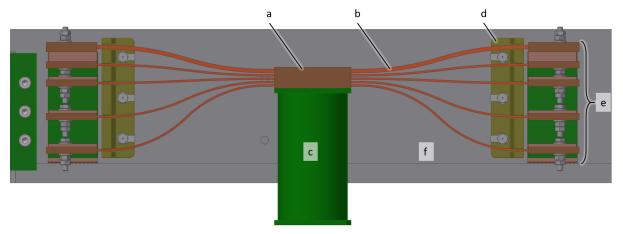

Fig. 3: Cold bus installation model front view with cold finger seat (a), flexible copper links (b), cold bus support (c), vibration damper (d), end connection geometry (e) and HTS-coil casing (f).

The use of flexible connectors between the rigid centre- and end pieces (as seen in Fig. 3) of the copper cold bus is necessary since the coil must be able to move up- and downwards as described in the previous paragraph. This is imperative because the centrepiece (Fig. 3 a) is fixed in its position via the G10 support strut. The strut, at its bottom end, is bolted into the vacuum vessel. Additionally, the flexible links allow for the compensation of thermal expansion of the coil and the copper connectors themselves. The cryocooler, which is not displayed in Fig. 3, presses onto said centrepiece with its second stage copper cylinder. This connection, however, is designed to be loose, allowing for a disconnection of the cold head and the cold bus centrepiece without breaking the cryostat vacuum.

3.2   Heat Load Approximation

This section deals with the approximation methods of heat loads on the thermal shield and the HTS-coil exclusively. The imperative cryostat design task of mechanical stress approximation is not part of this contribution.

As we mentioned in section 2.2, the thermal shield around the HTS-coil is actively cooled by the cryocooler's first stage while the coil itself is kept at ca. 25 K by the cooling power of the second stage. We had to consider the intrinsic cooling power limitation of cryocoolers. Therefore, throughout the cryostat design process, we approximated the expected heat loads on both stages of the cryocooler with every design iteration.

The theoretical background equations of these heat load calculations are well-known and can i.e. be found in [6]. In operational conditions, we are aiming for a vacuum in the order of 10^{-5} mbar inside the cryostat. This will be achieved by first pumping on the cryostat up to a residual pressure of 10^{-3}...10^{-4} mbar and afterwards cryopumping by means of the cryocooler. Thus, in the operational steady-state, heat transferred via condensation of gas molecules on cold surfaces and cryo-adsorption can be assumed negligibly small i.e. against the contribution of thermal radiation. An exemplary, manual calculation of heat conduction through the gaseous phase on the cold mass at a pressure of this order revealed the same outcome. This is why the approximations' focus lay exclusively on three heat load types: heat conduction through solid bodies ($\dot{Q}_{solid}$), thermal radiation ($\dot{Q}_{rad}$), and Joule heating ($\dot{Q}_{Joule}$).

To improve the thermal shield insulation against heat radiation, we will wrap all parts on the 80 K-level otherwise directly exposed to surfaces at room-temperature in multilayer insulation (MLI). This also allows us to manually provide a conservative approximation of the heat radiation by using the upper-end value of the heat transfer benchmark ($\dot{q}_{\mathrm{MLI}(300...80\,\mathrm{K})} \approx 1...2$ Wm^{-2}) determined by Lehmann [7].

The benchmark for $\dot{q}_{\mathrm{MLI}(80...4\,\mathrm{K})}$, whose temperature levels are sufficiently close to the 80...25 K we foresee in the induction heater, is much lower (≈ 0.15 Wm^{-2}). Plus, the distances between the thermal shield at 80 K and the HTS-coil at 25 K were in the order of tens of millimeters due to the spatial constraints of the whole cryostat explained in section 2.1. This combination of a small potential benefit versus the risk to cause a thermal short cut led us to the decision to dispense with an approach to insulate the 25 K-coil with MLI as well. Instead, we will have the surface of the coil casing made out of stainless steel electropolished to reduce its emissivity which leads to a smaller residual emissivity e$_r$ in eq. (1) and thus a decrease in radiation heat load.

$$\dot{Q}_{\mathrm{rad}} = e_{\mathrm{r}} \cdot A_{\mathrm{cold}} \cdot \sigma \cdot (T_{\mathrm{warm}}^4 - T_{\mathrm{cold}}^4) \qquad (1)$$

Eq. (1) shows the calculation of $\dot{Q}_{\mathrm{rad}}$ when assuming that the cold surface ($A_{\mathrm{cold}}, T_{\mathrm{cold}}$) is entirely surrounded by the warm surface ($A_{\mathrm{warm}}, T_{\mathrm{warm}}$) and the respective bodies are grey bodies [8]. Given the cryostats setup, in which a high-purity aluminum shield will surround the HTS-coil as thoroughly as possible, these conditions can be well assumed. On the basis of this equation, we calculated the heat load on the 25 K-level manually.

Wolfram Mathematica

To approximate $\dot{Q}_{\mathrm{Joule}}$ and $\dot{Q}_{\mathrm{solid}}$ through geometrically simple bodies, we used Wolfram Mathematica® including an interface to the CryoComp® cryogenic materials and thermal properties database [9]. This allowed us to write design tools for specific parts such as the support struts presented in section 3.1 and parametrize boundary conditions for easier adjustment. Throughout the thermal and mechanical design process, this proved to be remarkably useful.

ANSYS® Steady-State Thermal Analysis

To approximate values for $\dot{Q}_{\mathrm{solid}}$ concerning bodies whose geometries could not be simplified sufficiently within reasonable bounds to be evaluated analytically, we used the steady-state thermal analysis-feature of ANSYS® Workbench. Again, CryoComp® served as the source for the required material data. For these more complicated bodies, ANSYS® also enabled us to approximate the temperature distributions in the induction heater's operational state. The most important example for this is the cold bus presented in Fig. 3 through which all heat loads onto the HTS-coil will have to be conducted to the cold finger. Therefore, we had to design it in a way so that the temperature gradient from the cryocooler seat to the HTS-coil connection geometries was small enough to provide a sufficiently low temperature for the superconductor. To approximate temperature distributions for cases like this, ANSYS® was our central tool.

4   Results

As we explained in the previous sections, the induction heater's cryostat designing was a dynamic process. Due to the foreseen application of an intermediate thermal shield, we were - within the margins of mechanical, spatial and installation feasibility - able to choose the heat load distribution between both temperature levels. Naturally, the driving factor for this was the adaptation to the distribution of cooling powers between the two stages of potentially eligible cryocoolers. Fig. 4 shows the respective results.
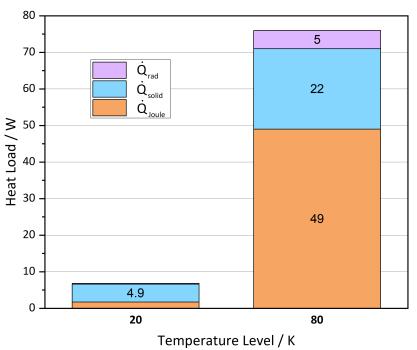

Fig. 4: Approximate expected heat loads by type on cryocooler stages at 20 K and 80 K during induction heater operation. Stacked from top to bottom for both temperature levels the contributions to the total heat loads are shown: thermal radiation, heat conduction through solids and Joule heating.

As Fig. 4 indicates, we expect the total heat load on the 20 K cryocooler stage to be around 6.8 W. Respectively, the different heat load types onto the 80 K-stage add up to ca. 76 W. $\dot{Q}_{\mathrm{Joule}}$ includes the heat conduction through the electric connectors because, along a live resistor with two different end temperatures, $\dot{Q}_{\mathrm{Joule}}$ and $\dot{Q}_{\mathrm{solid}}$ depend on each other. Goloubev [10] describes this in great detail. According to his descriptions, we minimized the sum of $\dot{Q}_{\mathrm{Joule}}$ and $\dot{Q}_{\mathrm{solid}}$ via the connectors by adequately choosing their length and cross-sectional area. Besides, we abstain from introducing error bars in Fig. 4 since we expect the unquantifiable inaccuracies caused by the simplification of geometries influencing all given heat load values to be far more significant than the material data uncertainties or numerical simulation errors. We address the issue of cooling power safety margins further in section 5.

Additionally, we want to point out the important fact here that Fig. 4 shows the heat loads expected during the induction heater operation. This means that the electric connection to the coil will be live. Accordingly, only in this state of the system, the exclusive Joule heating (ca. 20 W on 80 K and 0.9 W on 20 K) contributes to the total heat load. In the cooldown phase, respectively, when there is no electric current flowing, the only heat load contribution via the copper electric connections is heat conduction from the 300 K-end (ca. 29 W on 80 K and 0.8 W on 20 K). In both scenarios, the thermal shield receives the major part of the load since the electric connectors are thermalized on the 80 K-shield before reaching the coil at 25 K.

Naturally, as eq. (1) suggests, the contribution of $\dot{Q}_{\mathrm{rad}}$ increases for both stages during the cold mass and shield cooldown as T_{cold} drops. However, in comparison to the changes in $\dot{Q}_{\mathrm{Joule}}$, this effect is of small significance.

Regarding $\dot{Q}_{\text{solid}}$, we hardly expect any change by ramping up the coil current although the coil will only then experience a vertically directed electromagnetic force that needs to be supported (see section 3.1).

The whole heat load on the coil has to be withdrawn via the central piece of the cryostat, the cold bus. As mentioned in section 3.2, to investigate the resulting temperature gradient, we used the ANSYS® Steady-State Thermal Analysis software.
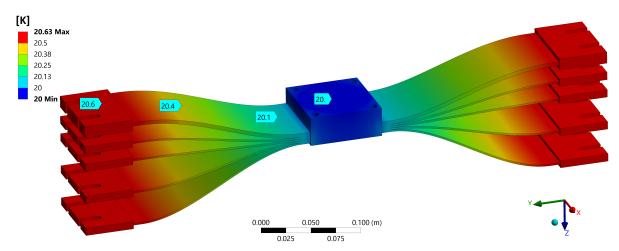

Fig. 5*:* ANSYS® Steady-State Thermal Analysis simulation result for our cold bus out of copper (RRR = 50). We applied a heat load of 6.8 W on the HTS-coil and 20 K cold head temperature.

Fig. 5 depicts the numerically determined temperature increase along our butterfly-shaped cold bus in the order of 600 mK between the cold finger contact surface on top of the centre piece and the HTS-coil's cold bus contact surfaces on either end. For this calculation, we provided ANSYS® with four major pieces of information. First, the part is exclusively composed of copper (RRR = 50). Second, we set the circular cold finger contact surface on top of the center piece to be at a constant temperature of 20 K. Third, the surfaces in contact with the HTS-coil's inner cold bus receive a heat flow of 6.8 W in total. This heat flow is distributed according to the cross-sectional area ratios of the single copper connectors. This means that almost half of the heat flow is conducted by the thicker top connectors. Fourth, we let ANSYS® treat all other surfaces as adiabatic. We are satisfied with the resulting temperature distribution that indicates a temperature of 20.6 K at the contacts to the HTS-coil's inner cold busses which will be made out of a single piece of OFHC-copper each. Accordingly, we expect the temperature increase along the coil to be sufficiently low as well. We want to point out the fact here, however, that we let ANSYS® treat the cold bus geometry shown in Fig. 5 as if it were a single piece of copper. In reality, the suppliers will have to fabricate the all end pieces and the centre part separately from the flexible strands.

5   Discussion

Cold Bus

In order to keep the temperature gradient shown in Fig. 5 sufficiently low despite of the mentioned manufacturing restrictions, we have foreseen two measures. Firstly, we experimentally determined the RRR-value of coppers used by various cold bus suppliers. This way, we were able to choose commercially available flexible E-Cu strands with RRR > 80, significantly exceeding the assumed RRR = 50 in our simulations (see Fig. 5) and thus providing a higher thermal conductivity. Secondly, we want to address the issue of having to have the cold bus made out of three separate copper pieces along each thermal path. The flexible strands will be pressed into massive copper sleeves at their ends. This alone, however, cannot guarantee a sufficiently good thermal contact. Therefore, we will apply a soft solder into the joints to increase the contact area between the strands and the sleeves. Eligible solder examples with high thermal conductivity at around 20 K are Sn63Pb37 and Sn60Pb40 [11].

Heat Load Distribution

The heat load depiction in Fig. 4 is one of the main results of our design process. Generally spoken, the cryostat design aims for the lowest heat loads possible on both stages. An important aspect of the design process, however, was to fit the distribution of said heat loads to both cryocooler stages according to the respective cooling

power distribution. One way to adjust the heat load distribution that can generally be applied is the thermalization of heat conducting bodies ($\dot{Q}_{\mathrm{solid}}$) using the thermal shield. This, in general, can shift a part of the heat load from the second (20 K) to the first stage (80 K) of the cryocooler. In particular, we will use this method on the major part of the coil support struts, the electric connection and sensor wiring. Another way to adjust the heat load distribution among both stages is via influencing $\dot{Q}_{\mathrm{rad}}$ from the thermal shield to the HTS-coil. The thermal shield is protecting the coil from thermal radiation from the inner vacuum vessel walls at 300 K by creating a surface of an intermediate temperature surrounding the cold coil. This decreases $\dot{Q}_{\mathrm{rad}}$ on the coil with respect to the thermal radiation it would receive from the 300 K-surface. To lower $\dot{Q}_{\mathrm{rad}}$ on the coil even further, we will have the surface of its stainless steel metal casing electropolished (values given i.e. by Kropschot [12]). Having the aluminum shield outer surface treated in the same way is not necessary due to the applied MLI. Decreasing the emissivity coefficient of the coil casing has a second, important advantage: Due to the lower $\dot{Q}_{\mathrm{rad}}$ during the unavoidable maintenance periods of the cryocooler, the coil will warm up slower. This allows for a faster re-cooldown to the ca. 25 K operating temperature, reducing the induction heater's maintenance downtime.

Cryocoolers

The heat load results provide the basis for the choice of a two-stage GM-cryocooler for the cooling power provision in our induction heater. As mentioned in section 3.2, in all aspects of the heat load approximation, the assumptions we made were conservative. Thus, for the theoretical induction heater model, a cryocooler providing 76 W of cooling power on the first stage at 80 K and 6.8 W at 20 K suffices. However, in our experience, there has to be another margin added to compensate for the non-ideal part manufacturing and apparatus assembly. We want to highlight again here, that, in order to design the induction heater as commercially competitive as possible, we are intending to install the least costly (and thus, generally, least powerful) cryocooler possible. Accordingly, we conducted a market evaluation and are able to give three GM-cryocooler examples here. Apart from being, in our opinion, potentially eligible for the task regarding their cooling power, the durations of their maintenance processes are foreseen to be sufficiently low as well. Table 1 lists them.

Table 1: Eligible GM-Cryocoolers at 20 K (2nd Stage) and 80 K (1st Stage) as given by the respective manufacturer

Manufacturer	CSIC Pride Cryogenic Technology Co., Ltd.	Leybold GmbH	Sumitomo Heavy Industries, Ltd.
Cold Head Model	KDE412SA	COOLPOWER 10 MD	CH-210L
He-Compressor Model	KDC6000V	COOLPAK 6000 HMD	F-70L
Min. 1st Stage Cooling Power / W	95	110	90
Min. 2nd Stage Cooling Power / W	15	18	9.5

Table 1 also shows that, we can, in fact, expect to be able to cool the induction heater efficiently via a single cryocooler. This is, because among all listed cryocooler models, the additional cooling power margins are at least 18 % (first stage, CH-210L) and 40 % (second stage, CH-210L). We want to point out here that the cooling power values given for the CH-210L is provided by the manufacturer at a temperature combination of 15 K and 65 K. However, these are the guaranteed values closest to our conditions available to us. Thus, we will set up an experimental test stand with which we will check the cooling capacities of different cryocoolers. The different cryocooler models differ not only in their cooling capacities but also in the cold head's dimensions. To maintain flexibility regarding the cryocooler choice nevertheless, we have designed the cold head seat in the cryostat in such a way that different models can be installed with minor changes in the attachment assembly. Furthermore, it is a convenient property in the scope of potential future upscaling-propositions of our induction heater.

6   Symbols and Abbreviations

Symbols

A	Area ($\mathrm{m^2}$)	
e_r	Residual Emissivity (-)	
$\vec{g}$	Earth's Gravity Constant ($\mathrm{m \cdot s^{-2}}$)	
$\dot{Q}$	Heat Flow (W)	
T	Temperature (K)	
σ	Stefan-Boltzmann Constant ($\mathrm{J \cdot m^{-2} \cdot s^{-1} \cdot K^{-4}}$)	

Abbreviations

BMWI	German Federal Ministry for Economic Affairs and Energy
CAD	Computer-Aided Design
EM	Electromagnetic
GM	Gifford-McMahon
HTS	High-Temperature Superconductor
MLI	Multilayer Insulation
RRR	Residual-Resistivity Ratio

7   References

[1]   German Environmental Award of the German Federal Environmental Foundation (DBU) 2010 [Online]. Available: https://www.dbu.de/123artikel29531_2418.html, Accessed last: Oct. 31, 2020

[2]   Gesamtverband der Aluminiumindustrie e.V., Jahresbericht 2019. Available: http://www.aluinfo.de, Accessed last: Nov. 5, 2020

[3]   Shepard, J., Zenergy Power Completes Successful Operation of First Commercial High-Temperature Superconductive (HTS) Induction Heater, EETech Media, LLC. (07/28/2008)

[4]   Choi, J., Design and Operational Test of Large-sized HTS Magnets with Conduction Cooling System for a 300 kW-class Superconducting Induction Heater, Energy Materials and Technologies, 2018, Vol. 3 Issue 54, 3189-3200

[5]   Neumann, H., Busch, L., Lietzow, R. and Noe, M., Advantages and disadvantages of an actively cooled thermal shield for a superconducting induction heater, Applied Superconductivity Conference Proceedings 2020 (in publication)

[6]   Frey, H., Eder, F. X. and Haefer, R. A., Tieftemperaturtechnologie. VDI, Düsseldorf, 1981

[7]   Lehmann, W., Superisolation (SI) – deren Qualität und Degradierung bei Anwendungen in der Kryotechnik, DKV-Tagungsbericht, Vol. 1, 99-117, Bremen, November 2000

[8]   Gröber, W., Erk, S., Grigull U., Die Grundgesetze der Wärmeübertragung, Springer, 2013

[9]   CryoComp Rapid Design Thermal Analysis Software. Eckels Engineering Inc. 1993-2017 [Online]. Available: http://www.eckelsengineering.com/, Accessed last: Oct. 18, 2020

[10]   Goloubev, D., Kühlung eines resistiven HTSL-Kurzschlussstrombegrenzers mit einer Gemisch-Joule-Thomson-Kältemaschine, PhD Thesis, Technische Universität Dresden, 2003

[11]   Bagrets, N., Barth, C. and Weiss, K.-P., Low Temperature Thermal and Thermo-Mechanical Properties of Soft Solders for Superconducting Applications, in: IEEE Transactions on Applied Superconductivity, Vol. 24, No. 3, 2014

[12]   Kropschot, R.H., Insulation Technology, in: Cryogenic Technology, John Wiley and Sons, Inc., 1963